Synthesis, Electrochemical Behavior, and Electronic Properties of Hyperbranched Poly(*p*-methylenetriphenylamine): An Unexpected Condensation Polymerization from *N*-[4-(Tosyloxybutyloxymethyl)-phenyl]-*N,N*-diphenylamine

Kun-Rung Lin,[†] Ying-Hsueh Chang Chien,[§] Chin-Chuan Chang,[§] Kuo-Huang Hsieh,*[,†,‡] and Man-kit Leung*[,†,§]

Institute of Polymer Science and Engineering, Department of Chemical Engineering, and Department of Chemistry, National Taiwan University, 1 Roosevelt Road, Section 4, Taipei 106, Taiwan, ROC

Received January 17, 2008; Revised Manuscript Received April 7, 2008

ABSTRACT: *N*-[4-Tosyloxybutyloxymethyl]phenyl]-*N,N*-diphenylamine showed unexpected chemical reactivity and polymerized to form hyperbranched poly(*p*-methylenetriphenylamine) (PMTPA) under neat conditions. The hyperbranched PMTPA was electrochemically active and could be deposited on electrode surface when oxidized. The SEM study revealed that electropolymerization of PMTPA would form uniform coating on ITO surface. Polymeric light-emitting diodes (PLEDs) employing the electroactive hyperbranched PMTPA as hole-transport layer in ITO/electrochemically polymerized HTL/EML(PVK-PBD-Ir(ppy)$_3$)/Mg/Ag demonstrated the brightness over 20 000 cd/m^2 and low turn-on voltage. In particular, the device performance was very steady regardless of the thickness of the PMTPA layer, ranging from 4 to 10 nm.

Introduction

The family of triphenylamine (TPA) derivatives has attracted intense research interest during the past few decades due to their excellent charge transporting properties.[1] Most of these hole-transport materials are small organic molecules. For example, devices using *N,N*′-bis(1-naphthyl)-*N,N*′-diphenylbenzidine (α-NPB) as the hole-transport layer (HTL) could be fabricated through thermal vapor deposition on the substrate under high-vacuum conditions.[2] On the other hand, polymeric hole-transport materials are attractive due to their high mechanical strength and thermal stability. Some problematic phenomena for molecular organic materials such as phase separation or crystallization from the amorphous film seldom occur in polymeric films. By taking the advantages of their high mechanical strength, morphological stabilities, and good processability, polymeric materials benefit for applications in flexible large-area panel displays.[3] Therefore, triphenylamine-based conjugated polymers have become extremely important targets to develop and explore. For example, TPA moieties had been covalently linked onto PPV backbones, which showed good electroluminescent performance due to effective charge injection and migration.[4a,b] Conjugated Schiff base polymers, prepared from condensation of 4,4′-diamino-substituted triphenylamine and dialdehydes, showed noncrystalline morphology, high heat resistance, and good hole-transport ability.[4c]

On the other hand, because of their high solubility in various organic solvents, TPA-based nonconjugated polymers are also good candidates to study. TPA units could be incorporated into nonconjugated polymer main chains[5] or hooked onto the side chains.[6] These materials showed high application potential as hole-transport materials. For example, linear nonconjugated polymers with hole-transport components along the backbone were prepared by condensation polymerization of either *N,N*′-di(4-tolyl)-*N,N*′-diphenylbenzidine (TPD) with aldehydes[5a] or alkyl-TPD with dihalides using Friedel−Crafts reactions.[5b] Photoconducting polymers in which TPD compounds were covalently linked through flexible oligomethylene glycol spacers in the main chain by Ullmann reaction have been reported.[5c] On the other hand, numerous nonconjugated polymers with TPA as the pendant groups were also synthesized. For instance, poly(norbornene)-based polymers with pendant TPA groups have been made by ring-opening metathesis polymerization. The polymers exhibited excellent device performance.[6a] Hole-injection polymers could also be synthesized by radical polymerization of methacrylate-based TPA. Electrochemical deposition of TPA or carbazole derivatives directly on ITO anode provided another entry for hole-transport layer fabrication.[6b]

Compared to the linear polymers mentioned above, hyperbranched polymers are alternatively outstanding candidates for scientific and industrial applications due to their unusual chemical and physical properties.[7,8] It has been reported that electrooptical devices with hyperbranched polymers showed significantly improved stability and efficiency in comparison to those with linear polymers.[9]

Recently, we have been interested in developing triphenylamine derivatives for PLED applications.[10] We have focused on *N*-[4-tosyloxybutyloxymethyl]phenyl]-*N,N*-diphenylamine (**1**) because it contained a reactive tosylate group. We expected that **1** could be conveniently hooked onto other polymers as pendant groups through substitution reaction to form new types of hole-transport material. However, we discovered that **1** showed

Scheme 1. Synthesis of PMTPA (2)

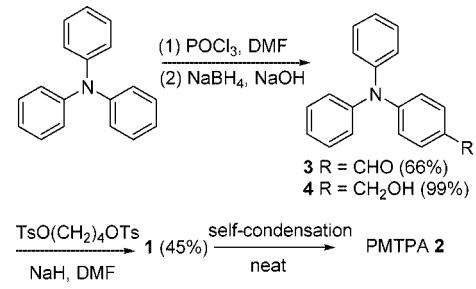

* To whom all correspondence should be addressed: Tel +886-2-33661673; Fax +886-2-23636359; e-mail mkleung@ntu.edu.tw; khhsieh@ntu.edu.tw.
[†] Institute of Polymer Science and Engineering.
[‡] Department of Chemical Engineering.
[§] Department of Chemistry.

10.1021/ma800127v CCC: $40.75
Published on Web 05/29/2008

unexpected chemical reactivity and would self-condense to form hyperbranched poly(*p*-methylenetriphenylamine) (PMTPA) (**2**). Herein, we report the synthesis, characterization, and electrochemical behavior of hyperbranched PMTPA (**2**) and its application to polymeric light-emitting diodes.

Chart 1

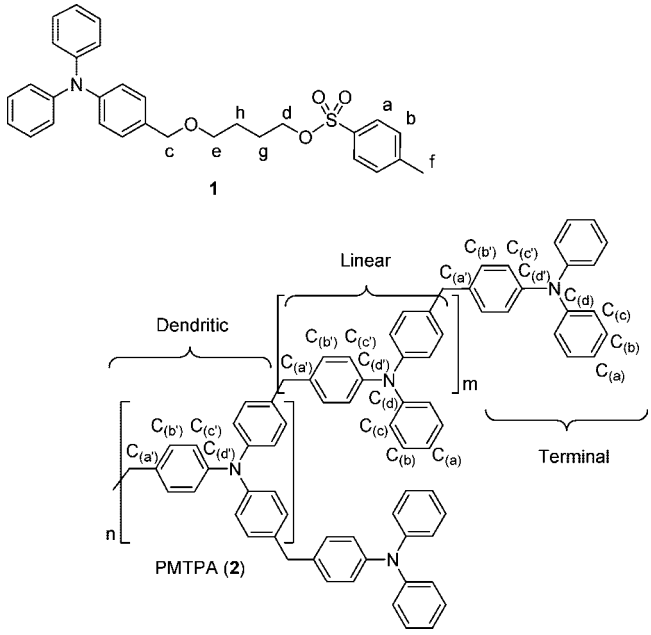

Experimental Section

***N*-[4-Tosyloxybutyloxymethyl]phenyl]-*N*,*N*-diphenylamine (1) and Polymer 2 (PMTPA).** A two-necked flask was charged with prepurified NaH (0.41 g, 16.9 mmol) and DMF (10 mL). A solution of **4** (4.2 g, 15.4 mmol) in DMF (10 mL) was added. After being stirred for a while, 1,4-butane ditosylate (11.0 g, 27.6 mmol) was then added and reacted at room temperature for 2 days. Methanol was added to quench the reaction. Methanol and part of the DMF were first removed by rotary evaporation. The residue was then washed with water and extracted with CH_2Cl_2. The crude product obtained was purified by column chromatography (silica gel, ethyl acetate/hexane (1/3) as eluent) to yield **1** (3.5 g, 45%) as a slightly yellowish liquid. ^{1}H NMR (400 MHz, $CDCl_3$): δ 7.76 (d, J = 8.4 Hz, 2H), 7.30 (d, J = 8.4 Hz, 2H), 7.19−7.21 (m, 4H), 7.13 (d, J = 8.4 Hz, 2H), 6.97−7.06 (m, 8H), 4.36 (s, 2H), 4.03 (t, 6 Hz, 2H), 3.42 (t, 6 Hz, 2H), 2.41 (s, 3H), 1.73−1.76 (m, 2H), 1.60−1.65 (m, 2H). The compound gradually polymerized when it was allowed to stand overnight to give PMTPA (**2**). The ^{1}H and ^{13}C NMR were discussed in the following section. The molecular weight distribution of the PMTPA was measured by gel permeation chromatography (Waters GPC System installed with two GPC columns of Styragel HR2 and Styragel HR4E that covered the range of M_n: 50−100 000) against polystyrene standards: M_w = 10 200; M_n = 3400; DPI = 3.01. Anal. Calcd for $C_{19}H_{15}N$, the molecular formula of the repeating unit: C, 88.68; H, 5.88; N, 5.44. Found: C, 85.39; H, 5.85; N, 5.16.

Electrochemical Deposition of HTL Films. Electropolymerizations of poly(4-vinyltriphenylamine) (PVTPA)[11,12] and poly(*p*-methylenetriphenylamine) (PMTPA) (5 mg) were carried out by cyclic voltammetry (0−1.5 V; 100 mV/s) with a three-electrode cell in CH_2Cl_2 containing tetrabutylammonium perchlorate (TBAP, 0.1 M) as the supporting electrolyte. A platinum wire was used as the auxiliary electrode, and Ag/AgCl (saturated) couple functioned as the reference electrode. The polymeric film obtained on ITO-coated glass electrode was rinsed with CH_2Cl_2 and dried before use. The film thickness was monitored by using Surfcorder ET3000 profilometer.

EML and Metal Cathode Formation. A solution of PVK, PBD, and Ir(ppy)$_3$ (PVK:Ir(ppy)$_3$:PBD = 100 mg:30 mg:40 mg) in $CHCl_3$ (8 mL) was prepared and allowed to stand on the bench for several hours to ensure complete dissolution of the materials. Dust and insoluble particles were removed by microfiltration before spin-coating. A membrane filter with channel size of 0.45 μm was used in the filtration. The polymeric solution was spin-coated onto the pretreated substrate, which contained a layer of eletropolymerized HTL on the ITO anode, at 3000 rpm for 90 s and dried under vacuum for 10 min at 70 °C. The metallic cathode composed of Mg and Ag was deposited onto the ITO/HTL/polymer system at pressure below 5 × 10^{-6} Torr. The deposition rates for the Mg and Ag cathodes were 1 and 4 Å/s, respectively, giving an active area of 0.126 cm^2, together with thickness up to 10 and 100 nm, respectively.

Scheme 2

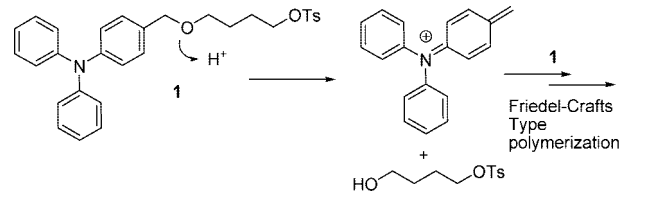

Results and Discussion

Preparation of PMTPA (2). As shown in Scheme 1, formulation of triphenylamine under Vilsmeier−Haack conditions[13] gave **3**, which was further reduced to benzylic alcohol **4**.[14] Alkylation of **4** with excess 1,4-butane ditosylate[15] gave the monotosylate precursor **1**. The monotosylate **1** was purified by liquid chromatography on silica gel, using EtOAc/hexane (1/3) as eluent. The pure monotosylate **1** was first isolated as a liquid but solidified if it was allowed to stand overnight. The ^{1}H and ^{13}C NMR study revealed that polymerization of **1** occurred to give hyperbranched PMTPA (**2**) as solid.

Since it was known that Friedel−Crafts type condensation polymerization of triphenylamine with carbonyl compounds would occur under acid-catalyzed conditions,[5a,b,16] one might suspect that the present polymerization was induced by any acidic impurity through similar mechanisms. However, this possibility was unlikely because the polymerization still proceeded smoothly even after neutralization with aqueous $NaHCO_3$. We therefore proposed that catalytic amounts of *p*-toluenesulfonic acid might be generated through partial hydrolysis of the *p*-tosylate group on **1** that further catalyzed the polymerization to give **2** (Scheme 2).

Anyway, this observation intrigued us to trace the polymerization reaction carefully by ^{1}H NMR spectroscopy (Figure 1). During the course of the polymerization, the growth of the broad resonance signal at 3.70−3.80 ppm, corresponding to the formation of $-ArCH_2Ar-$ during polymerization, was observed. The polymerization proceeded so fast that signals of the $-ArCH_2Ar-$ could be clearly observed even only 10 min after being concentrated. Parallel to the growth of the polymer, the signals (**c**, **d**, and **e**) of **1** at 4.36 (s, $-ArCH_2O-$), 4.03 (t, $TsOCH_2-$), and 3.42 (t, $-OCH_2-$) gradually faded away. Monomer **1** was completely consumed after being allowed to stand for 20 h. The byproduct, $HO(CH_2)_4OTs$, was identified after purification (Figure 1, spectrum 6). Since the $HO(CH_2)_4OTs$ is soluble in CH_3CN, it could be dissolved in CH_3CN and isolated from the insoluble polymer by filtration. The insoluble polymer was collected as white powder. Polymer **2** showed four sets of resonance signals, including two major aromatic signals at 7.1−7.2 ppm, 6.9−7.1 ppm, a small shoulder aromatic band at ~6.7 ppm, and one methylene band at 3.7−3.8 ppm (Figure 1, spectrum 5). The alkyl/aromatic integration ratio was in good agreement with the structure of poly(*p*-methylenetriphenylamine). The proposed skeleton was further supported by the MALDI mass analysis that showed clearly the fragmentation pattern of sequentially lost of the repeating unit (Figure

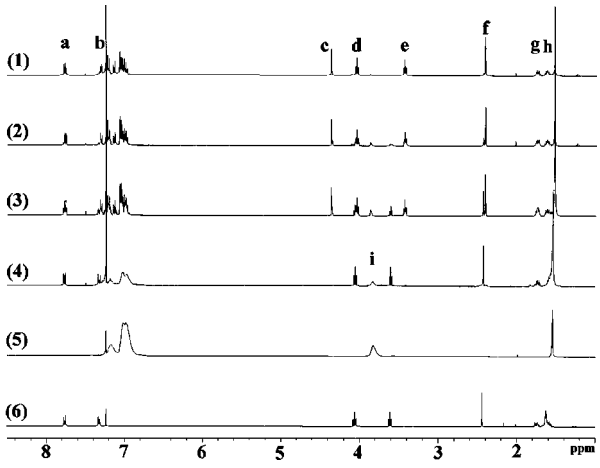

Figure 1. ^{1}H NMR trace for the growth of polymer **2** from **1**. The ^{1}H NMR spectra of the monomer **1** were sampled at different time during the progress of the polymerization: (1) 10 min after concentration, (2) 100 min after concentration, (3) 190 min after concentration, (4) 20 h after concentration, (5) ^{1}H NMR spectrum of PMTPA, and (6) ^{1}H NMR spectrum of $HO(CH_2)_4OTs$.

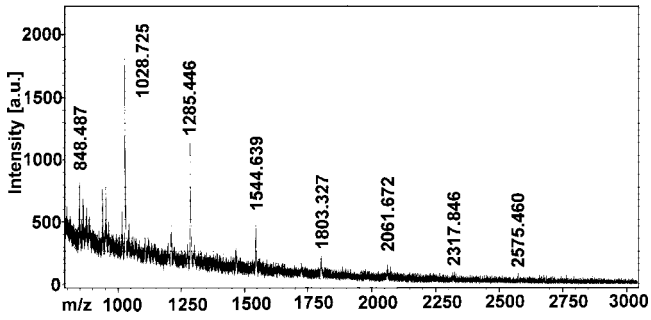

Figure 2. MALDI mass analysis of **2**.

2). Although monomer **1** might act as an AB_2-type precursor that would lead to a hyperbranched structure, the resolution of the ^{1}H NMR was not good enough to identify the composition of the terminal, linear, and dendritic units. However, the ^{13}C NMR analysis provided us well-resolved spectral data for the structural assignments.

To assign the spectral data for polymer **2**, the ^{13}C NMR of the authentic samples of Ph_3N, Ph_2N(*p*-tolyl), PhN(*p*-tolyl)$_2$, and N(*p*-tolyl)$_3$ were collected as standards for comparison (Table 1). A similar approach was adopted for characterization of the polymer from the Friedel−Crafts condensation reaction of triphenylamine and formaldehyde.[16] Ph_3N showed four sets of ^{13}C signals at 147.62, 129.02, 123.98, and 122.49 ppm. The resonance signal at 147.62 ppm was arising from the ipso carbon connected to the nitrogen atom, denoted as $C_{(d)}$.[17] Tritolylamine, (*p*-tolyl)$_3$N, showed four sets of aromatic ^{13}C signals at 145.51, 129.57, 123.72, and 131.58 ppm and a methyl signal at 20.87 ppm. The ipso carbon adjacent to the nitrogen atom, denoted as $C_{(d')}$, appeared at 145.51 ppm, was about 2.1 ppm upfield shifted than that of Ph_3N. On the other hand, affected by the methyl substituent, the signal of the ipso $C_{(a)}$ shifted to 131.58 ppm. Ph_2N(*p*-tolyl) showed eight aromatic ^{13}C signals, which could be divided into two groups. The first group of signals that appeared at 147.84, 128.96, 123.47, and 122.08 ppm was assigned to the phenyl carbons, denoted as $C_{(d)}$, $C_{(b)}$, $C_{(c)}$, and $C_{(a)}$, respectively. The second group of signals that appeared at 145.07, 132.58, 129.77, and 124.80 ppm was assigned to the tolyl carbons of $C_{(d')}$, $C_{(a')}$, $C_{(b')}$, and $C_{(c')}$, respectively. Since there are two phenyl groups on Ph_2N(*p*-tolyl), their signal intensities were almost 2 times higher than that of the tolyl groups. Similarly, PhN(*p*-tolyl)$_2$ also showed eight aromatic ^{13}C signals. The first group of signals that appeared at 148.02, 128.84, 122.78, and 121.54 ppm was assigned to the phenyl carbons, denoted as $C_{(d)}$, $C_{(b)}$, $C_{(c)}$, and $C_{(a)}$, respectively. The second group of signals that appeared at 145.24, 132.00, 129.59, and 124.26 ppm was assigned to the tolyl carbons of $C_{(d')}$, $C_{(a')}$, $C_{(b')}$, and $C_{(c')}$, respectively. Since there is only one phenyl group on PhN(*p*-tolyl)$_2$, its signal intensity was one-half of the tolyl groups.

It is worth mentioning that the chemical shifts of the phenyl and tolyl carbons were slightly shifted, relying on the number of *para*-methyl substituents on the compounds. Their δ values are summarized in Table 1 for comparison. When the number of the tolyl substitutent increased, the δ values of $C_{(d)}$ and $C_{(d')}$ on the phenyl rings were gradually downfield-shifted. For example, δ of $C_{(d)}$ for Ph_3N, Ph_2N(tolyl), and PhN(tolyl)$_2$ were 147.62, 147.84, and 148.02, respectively. A shift of about 0.2 ppm was observed for each of the tolyl group being introduced. A similar downfield shift effect was also observed for $C_{(d')}$. On the contrary, the δ values of $C_{(a)}$ to $C_{(c)}$ and $C_{(a')}$ to $C_{(c')}$ were upfield-shifted when the *para*-methyl substituents were introduced. The shifts for $C_{(a)}$, $C_{(a')}$, $C_{(c)}$, and $C_{(c')}$ were about 0.4−0.7 ppm for each methyl group being introduced. However, the shifts for $C_{(b)}$ and $C_{(b')}$ were relatively small. The relationships between structure and chemical shift were useful for identification of the terminal, linear, and dendritic units in the hyperbranched PMTPA (**2**) in the following paragraph.

Figure 3shows the ^{13}C NMR of PMTPA (**2**) in $CDCl_3$. The assignments are summarized in Table 2. Eight sets of aromatic signals were observed. An additional set of methylene signals were observed at 40.6 ppm (see Supporting Information). The signals of C(a), C(b), C(c), and C(d) of the phenyl units appeared at (122.42, 122.17), (129.13, 129.08), (123.88, 123.59), and (147.88, 147.96), respectively. The signals were assigned by comparing the data against those of the standards in Table 1. Since the carbons of the phenyl groups would only appear either at the terminal (T) units or at the linear (L) units, splitting of the corresponding ^{13}C resonances into two bands was observed. On the other hand, since the $CH_2C_6H_4$ units might appear at the terminal, linear, or dendritic (D) units, each corresponding resonances of C(a′), C(b′), C(c′), and C(d′) split into three bands. The signals of (135.69, 135.48, 135.25), (129.66, 129.62, 129.57), (124.43, 124.21, 123.95), and 145.79, 145.86, 145.95) were assigned to C(a′), C(b′), C(c′), and C(d′) of the $CH_2C_6H_4$ units, respectively.

The assignments of each set of signals to T, L, and D units were achieved on the basis of the previous discussion about the substituent effects on the upfield−downfield shift relationships. For example, two signals of C(a) of the phenyl units on T and L were appeared at 122.42 and 122.17 ppm. Since the δC(a) of PhN(tolyl)$_2$ showed up at the upfield position while that of Ph_2N(*p*-tolyl) showed up at the downfield position, the upfield signal at 122.17 ppm was therefore assigned to C(a)(L) and the signal at 122.42 ppm was assigned to C(a)(T). By using this strategy, the spectrum could be completely assigned.

To obtain quantitative information about the ratio of the terminal, linear, and dendritic units through their integration, the pulse sequence of inverse gated decoupling[18] was employed for ^{13}C NMR experiments. In this experiment, the signal enhancement effects arising from proton to carbon polarization transfer during decoupling would be minimized. The degree of branching, defined as (D + T)/(D + L + T), was found to be 0.47 ± 0.02 according to their ^{13}C NMR integrations.

Thermal Properties of PMTPA and PVTPA. Table 3 summarizes the molecular weights and thermal properties of the PMTPA and PVTPA that were used in the present study. The PMTPA obtained had the weight-average molecule weight (M_w) of 10 200 and a polydispersity index of 3.01. The PMTPA

Table 1. ^{13}C NMR Chemical Shifts of the Ph_3N Derivatives as Reference

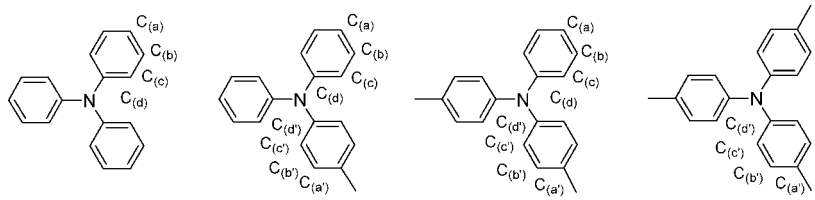

	carbon on the C_6H_5- rings				carbon on the $CH_3C_6H_4-$ groups			
	$C_{(d)}$	$C_{(b)}$	$C_{(c)}$	$C_{(a)}$	$C_{(d')}$	$C_{(b')}$	$C_{(c')}$	$C_{(a')}$
Ph_3N	147.62	129.02	123.98	122.49				
Ph_2N(*p*-tolyl)	147.84	128.96	123.47	122.08	145.07	129.77	124.80	132.58
PhN(*p*-tolyl)$_2$	148.02	128.84	122.78	121.54	145.24	129.59	124.26	132.00
N(*p*-tolyl)$_3$					145.51	129.57	123.72	131.38
δ shift[a]	(+)	(−)	(−)	(−)	(+)	(−)	(−)	(−)

[a] (+): downfield shifted; (−): upfield shifted.

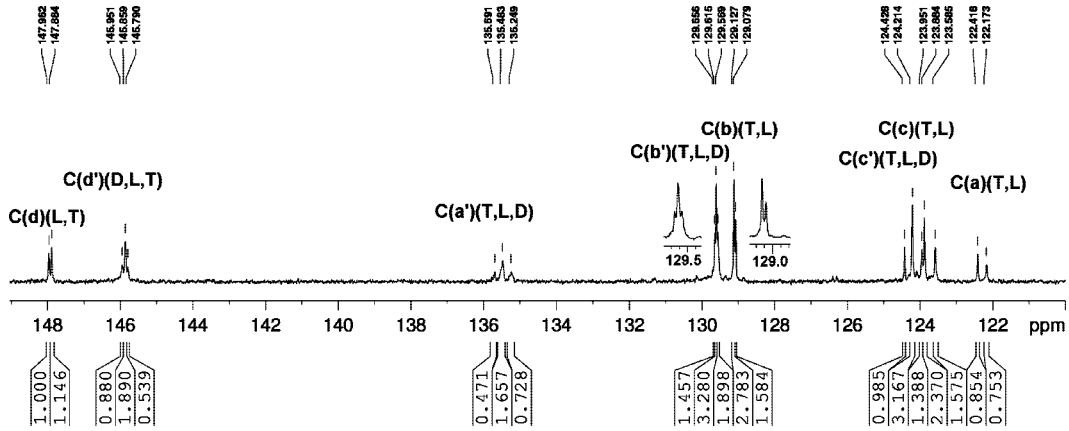

Figure 3. ^{13}C NMR spectra of the PMTPA (**2**).

Table 2. ^{13}C NMR chemical shifts of the PMTPA (2)

	carbon on the C_6H_5- rings					carbon on the $-CH_2C_6H_4-$ groups			
	C(d)	C(b)	C(c)	C(a)		C(d′)	C(a′)	C(b′)	C(c′)
terminal (T)	147.88	129.13	123.88	122.42		145.79	135.69	129.66	124.43
linear (L)	147.96	129.08	123.59	122.17		145.86	135.48	129.62	124.21
dendritic (D)						145.95	135.25	129.57	123.95
ratio (T/L)[a]	1/1.75[a]		1/1.60[a]	1/1.76[a]	(T/L/D)[b]	1/1.75/0.54	1/1.75/0.52		1/1.60/0.59

[a] The ratios were calculated according to their NMR integration: $0.5A_{(T)}/A_{(L)}$. [b] The ratios were calculated according to their NMR integration: $A_{(T)}/0.5A_{(L)}/0.333A_{(D)}$.

Table 3. Characterization and Thermal Properties of PMTPA and PVTPA

	M_w[a,d]	PDI[a]	T_g[b,d] (°C)	T_d[c,d] (°C)
PMTPA	10 200	3.01	158 ± 4	516 ± 4
PVTPA	13 034	2.02	133 ± 1	356 ± 6

[a] From GPC and calibrated against polystyrene standards. [b] By DSC at a heating rate of 10 °C/min under nitrogen. [c] With annealing pretreatment and temperature determined at 5% weight loss under nitrogen. [d] See Supporting Information for details.

exhibited a much higher onset weight-loss temperature (T_d at 5% weight loss) of 516 °C in comparison to PVTPA that showed a lower T_d of 356 °C. The higher T_d of PMTPA was attributed to the nonstyryl type hyperbranched structure. It has been known that main-chain skeleton of polystyrene would thermally decompose at around 350−380 °C.[19] Therefore, one might expect that PVTPA containing a polystyryl main chain would also decompose in a similar way at lower temperature.

The high glass-transition temperature (T_g) of 158 °C for PMTPA (**2**) was recorded, which is 25 °C higher than that of PVTPA. The high-T_g properties of **2** attracted us to further evaluate its potential for organic electronic applications. It has been known that EL devices with hyperbranched structures would have advantages of much improved stability and efficiency over those conventional linear polymers.[9d] These attracted us to investigate the possibility of using the present polymers for PLED applications. In the following section, the electrochemical deposition of PMTPA and its application for PLED devices were described.

Electrochemical Characteristics. The electrochemical studies were performed using cyclic voltammetry. In the first CV scan of PMTPA, an anodic wave peaked at 1.04 V was observed, which was attributed to the electrochemical oxidation of the triphenylamine pendant groups. However, two waves were shown in the backward scan, indicating the formation of the benzidine units through oxidative coupling of the triphenylamine pendant groups. This was further supported by the observation of a new wave at 0.81 V in the second or later scans, which was corresponding to the oxidation of the newly formed benzidine linkage. A pattern change with increasing current intensity was clearly observed in the repetitive CV studies. As shown in the inset of Figure 4, the anodic and cathodic current intensity increased that was linearly proportional to the number of CV scans.

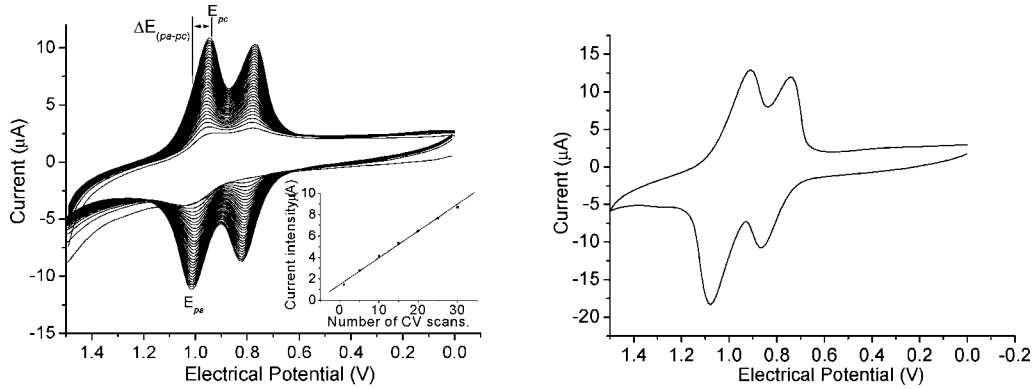

Figure 4. (left) Cyclic voltammograms of PMTPA with 30 repeated redox scan cycles (0−1.5 V; 100 mV/s, in a solution of TBAP in CH_2Cl_2). The inset shows a linear plot of the peak anodic current intensity at 0.82 V vs the number of CV cycles. (right) Cyclic voltammogram of electrochemically deposited PMTPA in the absence of the polymer precursor.

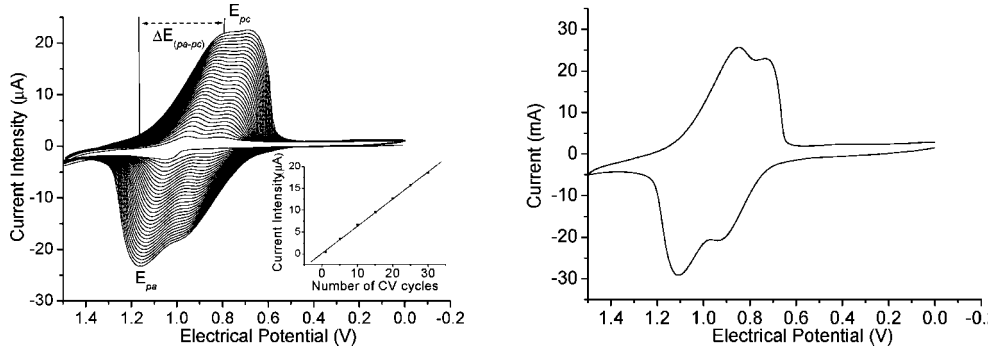

Figure 5. (left) Cyclic voltammograms of PVTPA with 30 repeated redox scan cycles. (right) Cyclic voltammogram of electrochemically deposited PVTPA in the absence of the polymer precursor.

Similar current intensity growth was also observed for PVTPA in repetitive CV studies (Figure 5), indicating that formation of benzidine units through electrochemical coupling had also effectively occurred for PVTPA. Again, the current intensity growth was also linearly proportional to the number of scans. This observation suggested that the electrochemical polymerization process could still effectively proceed even after 30 CV cycles. However, the separation between the E_{pc} and the E_{pa} was relatively large in comparison to that of PMTPA. This observation suggested that the electrode surface conditions for the electrochemical deposition process may be somewhat different between the two cases. This observation urged us to further study the film morphology by SEM in a later section.

Surface Work-Function Measurement. Surface work functions of the films were important parameters that governed the PLED device performance. The surface work functions were measured by using atmospheric photoelectron spectroscopy (Riken Keiki AC-2), from which we could also determine the ionization potentials (IPs) of the electrode surface, which would be referred to the energy level of the HOMO energy level of the electrode.

The studied films on ITO were prepared by electropolymerization. The films were rinsed with CH_2Cl_2 to remove the residual organic supporting electrolyte after electropolymerization. The work function of the modified ITO electrodes was then measured by AC-2 directly, and the data are summarized in Table 4. The HOMO energies were found ranging from −5.51 to −5.39 eV for PMTPA and −5.53 to −5.57 eV for PVTPA.

It is notable to point out that the HOMO energy of the ITO was significantly modified by the electrochemically deposited layer. Before surface modification pretreatment, the bare ITO has the HOMO value of −4.91 eV. However, after being coated with a very thin layer of PMTPA by five CV cycles, the HOMO energy dropped considerably to −5.51 eV. The HOMO value of the surface would then slightly increase from −5.51 to −5.39 eV when the thickness of PMTPA increased.

Table 4. HOMO Levels of Electrochemically Polymerized Films for Different Repeated Redox Scan Cycles

CV cycle numbers	PMTPA HOMO[a,b] (eV)	PVTPA HOMO[a,b] (eV)
5	−5.51	−5.53
10	−5.43	−5.57
20	−5.39	−5.56

[a] Determined by AC-2 measurement. [b] The work function of ITO is −4.91 eV.

A similar effect was also observed when the ITO surface was modified by electrochemical deposition of PVTPA. The HOMO value dropped from −4.91 eV to −(5.53−5.57) eV. However, the HOMO value did not vary much when the number of the CV cycles increased.

The HOMO values of −(5.4−5.6) eV for the electrochemically deposited PMTPA and PVTPA located right in between the HOMO of −4.91 eV for ITO and that of −6.10 eV for PVK.[20] The well-matched HOMO energy levels made these polymers appropriate materials for hole injection and transport purpose in PLED applications.

Device Performance. In the present study, we adopted a strategy of electrochemical deposition of PMTPA or PVTPA as the hole-injection and hole-transport layer on top of the ITO substrate. The light emissive layer of PVK-Ir$(PPy)_3$-PBD[21] was then spin-coated, followed by thermal vapor deposition of the active metal cathode. The PLED device performance is summarized in Tables 5 and 6.

The effects of the electrodeposited hole-injection layer on the turn-on voltage were definitely crucial. The performance of the device was found to be highly dependent on the existence of the HTL layer. Other examples of using polymeric hole-

Table 5. Dependence of the PLED Device Characteristics on the Thickness of Electrochemical Polymerized PMTPA HTL[d]

CV cycle numbers	HTL film thickness (nm)[a]	turn-on voltage (V) at 100 cd/m^2	max brightness (cd/m^2)	max efficiency (cd/A)
1	0[c]	N.A.[b]	N.A.[b]	N.A.[b]
3	0[c]	12.3 ± 0.26	16670 at 21 V	8.9
5	0[c]	11.9 ± 0.05	20110 at 22 V	8.9
10	0[c]	11.5 ± 0.05	21230 at 20 V	10.4
15	4.3	11.5 ± 0.20	18960 at 20 V	10.1
20	9.4	11.2 ± 0.05	27280 at 20 V	9.8
30	13.6	13.7 ± 0.20	5920 at 21 V	6.9
40	24.9	13.8 ± 0.10	2757 at 21 V	4.6

[a] From Surfcorder ET3000 profilometer. [b] No luminescence. [c] Too thin to measure polymeric film thickness. [d] A standard device of ITO/PEDOT:PSS/EML/Mg/Ag was employed as reference for comparison. The standard device showed a turn-on voltage of 12.5 V; with maximum brightness of 5036 cd/m^2 at 23 V and maximum efficiency of 22.5 cd/A.

Table 6. Dependence of the PLED Device Characteristics on the Thickness of Electrochemical Polymerized PVTPA HTL

CV cycle numbers	HTL film thickness (nm)[a]	turn-on voltage(V) at 100 cd/m^2	max brightness (cd/m^2)	max efficiency (cd/A)
1	0[c]	N.A.[b]	N.A.[b]	N.A.[b]
3	10.4	11.9 ± 0.05	22760 at 21 V	13.6
5	16.0	14.4 ± 0.05	21700 at 23 V	12.7

[a] From Surfcorder ET3000 profilometer. [b] No luminescence. [c] Too thin to measure polymer film thickness.

transport layer to improve the OLED device performance have been reported and discussed in the literature.[22]

Without being modified by the electrochemical coating, the performance of the device of bare-ITO/PVK-Ir(PPy)$_3$-PBD/Mg-Ag was poor.[23] This primitive PLED showed the turn-on voltage of 23 V, with the maximum brightness of 320 cd/m^2 and the current efficiency of 1.10 cd/A. However, when a layer of PMTPA was electrochemically deposited on ITO for three CV cycles, the hole-injection and hole-transport performance was highly improved so that the PLED device would be turned on at 12.3 V. The device performance would be further improved when the thickness of the HTL layer increased. The best devices were resulted when PMTPA were deposited repeatedly for 20 CV cycles, in which the thin-film thickness was around 10 nm. The superior hole-injection and transport capability of the layer significantly reduced the turn-on voltage of the PLED to 11.2 V, with the maximum brightness of 27 280 cd/m^2 and the current efficiency of 9.8 cd/A. Worthy to be mentioned was the steady device performance within a wide range of film thickness distributed from 4 to 10 nm. Within this thickness range, the film thickness variations would not significantly affect the electronic characters of the device, and therefore the thickness deviation during electropolymerization could be tolerated. When the thickness of the PMTPA layer further increased over 10 nm, the hole-transport process through the polymer matrix became difficult, and the turn-on voltage increased.

PVTPA has higher deposition rate in comparison to PMTPA. After repeatedly scan for three CV cycles, the measured film thickness was about 10 nm. Again, the presence of the electrochemically deposited layer significantly improved the performance of the PLED device, with lower turn-on voltage and much higher brightness.

Surface Morphology Investigation into Electrodeposited HTL Films. To further understand the morphology of the electrochemically deposited thin films, films of PMTPA and PVTPA from electropolymerization were subjected to field-emission scanning electron microscopy (SEM) analysis. Figure 6 shows the top-view image of the films from PMTPA. The film thickness was highly uniform, and the morphology was homogeneous. Instead of having a continuous film surface, the

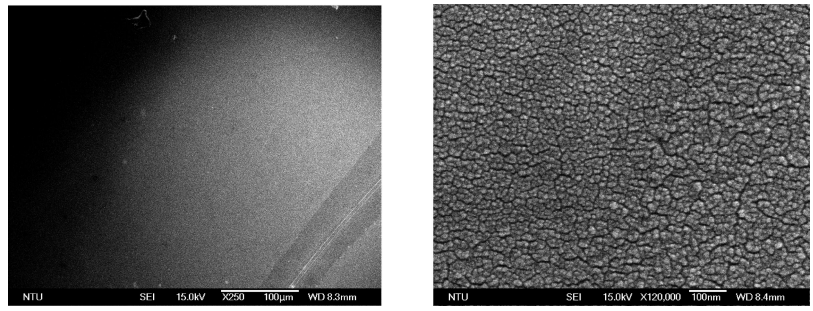

Figure 6. SEM picture of PMTPA film obtained by 40 CV cycles. The left picture showed a smooth surface from electrodeposition of the PMTPA-coated ITO glass. An artificial scratch was made at the right bottom corner. The right picture was an enlargement by 120K magnification of the central area.

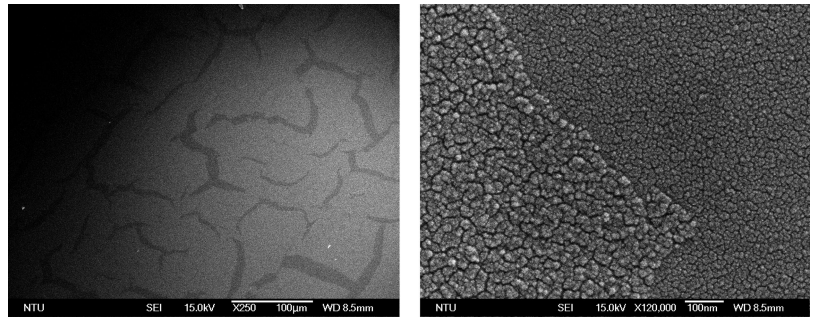

Figure 7. SEM picture of PVTPA film obtained by three CV cycles. The left picture showed the morphology of the PVTPA-coated ITO glass. Numerous cracks could be clearly observed. The right picture was an enlargement by 120K magnification of the crack area.

polymer layer was composed of granulates with the granule sizes of 10−20 nm. The sizes were close to that of the ITO granulates. Therefore, it is reasonable to propose that the hyperbranched PMTPA evenly grew along the surface of the ITO granulates. The morphology maintained during electropolymerization even after 40 CV cycles, with the film thickness up to 25 nm.

On the other hand, the thickness of the films from PVTPA was uneven. Numerous cracks were observed on the surface (Figure 7). The width of the cracks was around 5−20 μm. Although the mechanisms for the formation of cracks on the thin film of PVTPA are unclear, our preliminary SEM study revealed that it might be controlled by the chemical kinetics of the film growing. The rate of electrochemical polymerization on the coated areas is higher than on the bare ITO surface. The depth of the cracks increased when the number of the CV sweeps increased. The uneven distribution of the electroactive layer may lead to different electrochemical kinetics in various regions, leading to a broadening effect to the CV waves. Furthermore, as we mentioned before, the performance of hole-injection and transport layer was thickness dependent. The performance would reach to the maximum at around 10 nm thickness. The presence of the cracks would limit the effective paths for hole injection, leading to higher interfacial resistance for the device circuit and therefore increased the device turn-on voltage.

Conclusion

In summary, we demonstrate a new synthetic approach for PMTPA (**2**). Electropolymerization of the hyperbranched PMTPA would give rise to a highly homogeneous and tight surface. The colorless crack-free layer provided good hole injection and transport performance for PLED applications. This led to improved performance of the PLED, including low turn-on voltage and high brightness. Further investigations on the morphology of the electrochemically deposited thin-films are ongoing.

Acknowledgment. We thank the National Science Council of Taiwan (NSC 95-2113-M002-021-MY3), Academia Sinica (Thematic Project), the Ministry of Economic Affairs (grant 93-EC-17-A-08-S1-0015), Advanced Polymer Nanotechnology Research, and Ministry of Education of Taiwan for their financial and technical support.

Supporting Information Available: Synthetic procedures for **3** and **4**, ^{13}C NMR spectra of N(*p*-tolyl)$_3$, Ph$_2$N(*p*-tolyl), PhN(*p*-tolyl)$_2$, Ph$_3$N, original ^{13}C NMR spectra of polymer **2**, GPC, TGA, DSC, and brightness/voltage curves for the PLED devices. This material is available free of charge via the Internet at http://pubs.acs.org.

References and Notes

(1) (a) Loy, D. E.; Koene, B. E.; Thompson, M. E. *Adv. Funct. Mater.* **2002**, *12*, 245. (b) Shirota, Y. *J. Mater. Chem.* **2000**, *10*, 1. (c) Tanaka, H.; Tokito, S.; Taga, Y.; Okada, A. *Chem. Commun.* **1996**, 2175. (d) Adachi, C.; Nagai, K.; Tamoto, N. *Appl. Phys. Lett.* **1996**, *66*, 2679.

(2) (a) Tang, C. W.; VanSlyke, S. A. *Appl. Phys. Lett.* **1987**, *51*, 913. (b) Tang, C. W.; VanSlyke, S. A.; Chen, C. H. *J. Appl. Phys.* **1989**, *65*, 3610. (c) Niu, Y. H.; Liu, M. S.; Ka, J. W.; Jen, A. K. Y. *Appl. Phys. Lett.* **2006**, *88*, 093505. (d) Kuo, C.-H.; Lee, J.-H.; Leung, M.-k.; Hsieh, K.-H. *Chem. Mater.* **2006**, *18*, 4121.

(3) (a) Gu, G.; Shen, Z.; Burrows, P. E.; Forrest, S. R. *Adv. Mater.* **1997**, *9*, 725–728. (b) Tsutsui, T.; Fujita, K. *Adv. Mater.* **2002**, *14*, 949. (c) Yang, Y.; Huang, Q.; Metz, A. W.; Ni, J.; Jin, S.; Marks, T. J.; Madsen, M. E.; DiVenere, A.; Ho, S.-T. *Adv. Mater.* **2004**, *16*, 321. (d) Lee, K. J.; Motala, M. J.; Meitl, M. A.; Childs, W. R.; Menard, E.; Shim, A. K.; Rogers, J. A.; Nuzzo, R. G. *Adv. Mater.* **2005**, *17*, 2332. (e) Hide, F.; Díaz-García, M. A.; Schwartz, B. J.; Heeger, A. J. *Acc. Chem. Res.* **1997**, *30*, 430. (f) Greenham, N. C.; Friend, R. H. *Solid State Physics*; Enhrenreich, H., Spaepen, F., Eds.; Academic: San Diego, 1995; Vol. *49*, p 1. (g) Gustafsson, G.; Cao, Y.; Treacy, G. M.; Klavetter, F.; Colaneri, N.; Heeger, A. J. *Nature (London)* **1992**, *357*, 477. (h) Lin, K.-R.; Kuo, C.-H.; Leung, M.-k.; Hsieh, K.-H. *Eur. Polym. J.* **2007**, *43*, 4279.

(4) (a) Pu, Y. J.; Soma, M.; Kido, J.; Nishide, H. *J. Photopolym. Sci. Technol.* **2002**, *15*, 259. (b) Liao, L.; Pang, Y.; Ding, L.; Karasz, F. E. *Macromolecules* **2004**, *37*, 3970. (c) Niu, H.; Huang, Y.; Bai, X.; Li, X.; Zhang, G. *Mater. Chem. Phys.* **2004**, *86*, 33.

(5) (a) Son, J. M.; Mori, T.; Ogino, K.; Sato, H. *Macromolecules* **1999**, *32*, 4849. (b) Mori, T.; Strzelec, K.; Sato, H. *Synth. Met.* **2002**, *126*, 165. (c) Ostrauskaite, J.; Karickal, H. R.; Leopold, A.; Haarer, D.; Thelakkat, M. *J. Mater. Chem.* **2002**, *12*, 58. (d) Ohsawa, Y.; Ishikawa, M.; Miyamoto, T.; Murofushi, Y.; Kawai, M. *Synth. Met.* **1987**, *18*, 371.

(6) (a) Bellmann, E.; Shaheen, S. E.; Grubbs, R. H.; Marder, S. R.; Kippelen, B.; Peyghambarian, N. *Chem. Mater.* **1998**, *10*, 1668. (b) Kolb, E. S.; Gaudiana, R. A.; Mehta, P. G. *Macromolecules* **1996**, *29*, 2359. (c) Liu, S.; Jiang, X.; Ma, H.; Liu, M. S.; Jen, A. K. Y. *Macromolecules* **2000**, *33*, 3514. (d) Feast, W. J.; Peace, R. J.; Sage, I. C.; Wood, E. L. *Polym. Bull.* **1999**, *42*, 167. (e) Behl, M.; Hattemer, E.; Brehmer, M.; Zentel, R. *Macromol. Chem. Phys.* **2002**, *203*, 503. (f) Behl, M.; Zentel, R. *Macromol. Chem. Phys.* **2004**, *205*, 1633. (g) Compton, R. G.; Laing, M. E.; Ledwith, A.; Abu-Abdoun, I. I. *J. Appl. Electrochem.* **1988**, *18*, 431. (h) Cravino, A.; Roquet, S.; Aleveque, O.; Leriche, P.; Frere, P.; Roncali, J. *Chem. Mater.* **2006**, *18*, 2584. (i) Cravino, A.; Roquet, S.; Leriche, P.; Aleveque, O.; Frere, P.; Roncali, J. *Chem. Commun.* **2006**, *13*, 1416. (j) Deng, S.; Advincula, R. C. *Chem. Mater.* **2002**, *14*, 4073. (k) Advincula, R. C. *Polym. Mater. Sci. Eng.* **2006**, *94*, 271.

(7) (a) Kim, Y. H. *J. Polym. Sci., Part A: Polym. Chem.* **1998**, *36*, 1685. (b) Voit, B. *J. Polym. Sci., Part A: Polym. Chem.* **2000**, *38*, 2505. (c) Chang, H. T.; Fréchet, J. M. J. *J. Am. Chem. Soc.* **1999**, *121*, 2313. (d) Guan, Z. *J. Am. Chem. Soc.* **2002**, *124*, 5616. (e) Stiriba, S. E.; Kautz, H.; Frey, H. *J. Am. Chem. Soc.* **2002**, *124*, 9698.

(8) (a) Cao, C.; Yan, D. Y. *Macromolecules* **2003**, *36*, 613. (b) Xu, M. H.; Zhang, H. C.; Pu, L. *Macromolecules* **2003**, *36*, 2689. (c) Chen, J.; Peng, H.; Law, C. C. W.; Dong, Y.; Lam, J. W. Y.; Williams, I. D.; Tang, B. Z. *Macromolecules* **2003**, *36*, 4319. (d) Kang, S. H.; Luo, J.; Ma, H.; Barto, R. R.; Frank, C. W.; Dalton, L. R.; Jen, A. K. Y. *Macromolecules* **2003**, *36*, 4355. (e) Schmaljohann, D.; Komber, H.; Barratt, J. G.; Appelhans, D.; Voit, B. I. *Macromolecules* **2003**, *36*, 97.

(9) (a) Wang, F.; Wilson, M. S.; Rauh, R. D.; Schottland, P.; Reynold, J. R. *Macromolecules* **1999**, *32*, 4272. (b) Hua, J. L.; Li, B.; Meng, F. S.; Qian, S. X.; Tian, H. *Polymer* **2004**, *45*, 7143. (c) Meng, F. S.; Mi, J.; Qian, S. X.; Chen, K. C.; Tian, H. *Polymer* **2003**, *44*, 6851. (d) Paul, G. K.; Mwaura, A.; Argun, A. A.; Taranekar, P.; Reynolds, J. R. *Macromolecules* **2006**, *39*, 7789.

(10) (a) Chou, M.-Y.; Leung, M.-k.; Su, Y. O.; Chiang, C. L.; Lin, C.-C.; Liu, J.-H.; Kuo, C.-K.; Mou, C.-Y. *Chem. Mater.* **2004**, *16*, 654–661. (b) Leung, M.-k.; Chou, M.-Y.; Su, Y. O.; Chiang, C. L.; Chen, H.-L.; Yang, C. F.; Yang, C.-C.; Lin, C.-C.; Chen, H.-T. *Org. Lett.* **2003**, *5*, 839.

(11) Boiteau, L.; Moroni, M.; Hilberer, A.; Werts, M.; De Boer, B.; Hadziioannou, G. *Macromolecules* **2002**, *35*, 1543.

(12) (a) Deng, L.; Furuta, P. T.; Garon, S.; Li, J.; Kavulak, D.; Thompson, M. E.; Frechet, J. M. J. *Chem. Mater.* **2006**, *18*, 386–395. (b) Lindner, S. M.; Thelakkat, M. *Macromolecules* **2004**, *37*, 8832. The synthetic procedures were reported in their corresponding supporting information.

(13) Moon, K. J.; Shim, H. K.; Lee, K. S.; Prasad, P. N. *Macromolecules* **1996**, *29*, 861.

(14) Lee, J.; Jung, B. J.; Lee, J. I.; Chu, H. Y.; Do, L, M.; Shim, H. K. *J. Mater. Chem.* **2002**, *12*, 3494.

(15) Martin, A. E.; Ford, T. M.; Bulkowski, J. E. *J. Org. Chem.* **1982**, *47*, 412.

(16) Son, J.-M.; Nakao, M.; Ogino, K.; Sato, H. *Macromol. Chem. Phys.* **1999**, *200*, 65.

(17) Pretsch, E.; Seibl, J.; Simon, W.; Clerc, T. *Tables of Spectral Data for Structure Determination of Organic Compounds*, 2nd ed.; Springer-Verlag: Berlin, 1989; p C120.

(18) Silverstein, R. M.; Bassler, G. C.; Morrill, T. C. *Spectrometric Identification of Organic Compounds*, 5th ed.; Wiley: New York, 1991; p 250.

(19) (a) Muraki, T.; Ueta, M.; Ihara, E.; Inoue, K. *Polym. Degrad. Stab.* **2004**, *84*, 87–93. (b) Roland, A. I.; Schmidt-Naake, G. *J. Anal. Appl. Pyrolysis* **2001**, 58–59, 143.

(20) Yu, W.-L.; Pei, J.; Cao, Y.; Huang, W. *J. Appl. Phys.* **2001**, *89*, 2343.

(21) (a) Kohler, A.; Wilson, J. S.; Friend, R. H. *Adv. Mater.* **2002**, *14*, 701. (b) Beeby, A.; Bettington, S.; Samuel, I. D. W.; Wang, Z. *J. Mater. Chem.* **2003**, *13*, 80.

(22) Mutaguchi, D.; Okumoto, K.; Ohsedo, Y.; Moriwaki, K.; Shirota, Y. *Org. Electron.* **2003**, *4*, 49.

(23) Chiang, C. C.; Chen, H.-C.; Lee, C.-S.; Leung, M.-k.; Lin, K.-R.; Hsieh, K.-H. *Chem. Mater.* **2008**, *20*, 540.

MA800127V